Stability of laser-propelled wafer satellites

Prashant Srinivasan[a], Gary B. Hughes[b], Philip Lubin[c], Qicheng Zhang[c], Jonathan Madajian[c], Travis Brashears[c], Neeraj Kulkarni[c], Alexander Cohen[c], and Janelle Griswold[c]

prsriniv@calpoly.edu
gbhughes@calpoly.edu
lubin@deepspace.ucsb.edu

[a]Physics Department, California Polytechnic State University, San Luis Obispo, CA 93407-0405
[b]Statistics Department, California Polytechnic State University, San Luis Obispo, CA 93407-0405
[c]Physics Department, University of California, Santa Barbara, CA 93106-9530
[d]Aerospace Engineering Department, California Polytechnic State University, San Luis Obispo, CA 93407-0405

ABSTRACT

For interstellar missions, directed energy is envisioned to drive wafer-scale spacecraft to relativistic speeds. Spacecraft propulsion is provided by a large array of phase-locked lasers, either in Earth orbit or stationed on the ground. The directed-energy beam is focused on the spacecraft, which includes a reflective sail that propels the craft by reflecting the beam. Fluctuations and asymmetry in the beam will create rotational forces on the sail, so the sail geometry must possess an inherent, passive stabilizing effect. A hyperboloid shape is proposed, since changes in the incident beam angle due to yaw will passively counteract rotational forces. This paper explores passive stability properties of a hyperboloid reflector being bombarded by directed-energy beam. A 2D cross-section is analyzed for stability under simulated asymmetric loads. Passive stabilization is confirmed over a range of asymmetries. Realistic values of radiation pressure magnitude are drawn from the physics of light-mirror interaction. Estimates of beam asymmetry are drawn from optical modeling of a laser array far-field intensity using fixed and stochastic phase perturbations. A 3D multi-physics model is presented, using boundary conditions and forcing terms derived from beam simulations and light-mirror interaction models. The question of optimal sail geometry can be pursued, using concepts developed for the baseline hyperboloid. For example, higher curvature of the hyperboloid increases stability, but reduces effective thrust. A hyperboloid sail could be optimized by seeking the minimum curvature that is stable over the expected range of beam asymmetries.

Keywords: Directed Energy, Laser Propulsion, Interstellar Travel

1. INTRODUCTION

1.1. Background

Deep space missions, such as Voyager 1 (17.2 km/s) and New Horizons (16.26 km/s) are among the fastest human-made objects in existence. Final velocities of such vehicles are attained by a combination of propellant-driven boosters and gravity assist maneuvers. While these velocities are remarkable, Voyager 1 would still require 74 000 years to reach Alpha Centauri at its current velocity. For interstellar missions, directed energy is envisioned to drive wafer-scale spacecraft to relativistic speeds.[1-14] The spacecraft would include all mission components imbedded in a wafer, such as power, laser communications, photon-thruster or micro-reaction wheel attitude control system, imaging and other sensors. The driving force is provided by radiation pressure from a large array of phase-locked lasers, either in Earth orbit or stationed on the ground. The spacecraft includes a reflective sail, converting momentum from photons in the directed-energy beam into thrust.

Prior studies have explored requirements for propelling a wafer-scale spacecraft with a 1 m sail to ~0.26 c; travel time to α-Centauri would be approximately 15 years.[11-14] One critical issue with laser propulsion is attitude stability of the spacecraft: pointing jitter and intensity fluctuations from the laser will result in asymmetric flux on the spacecraft sail.[15] The spacecraft design must include passive righting mechanisms that compensate for asymmetric flux, maintaining the sail orientation approximately normal to the directed-energy beam during the acceleration phase. This paper combines models of laser phased-array beam formation with analysis of sail geometry to explore propulsion stability of laser-propelled wafer satellites.

Planetary Defense and Space Environment Applications, edited by Gary B. Hughes, Proc. of SPIE
Vol. 9981, 998105 · © 2016 SPIE · CCC code: 0277-786X/16/$18 · doi: 10.1117/12.2237715

2. SAIL GEOMETRY AND ASYMMETRIC RADIATION PRESSURE

2.1. Passive Stability Concepts

Sail geometry will be critical to propulsion. In an ideal scenario, the directed energy beam would arrive at the sail with uniform intensity. In this case, a flat sail would be optimal, because photons reflecting off the sail surface will impart a force on the sail in a direction normal to the sail surface. A flat reflective sail with a uniform, normal beam would result in maximum forward thrust. The ideal scenario of uniform intensity will never be attained, so there will nearly always be some amount of axial asymmetry in the force applied over the sail surface. With any amount of axial beam asymmetry, a flat sail will begin to yaw, with virtually no chance of recovery. To design a propulsion scheme that is robust to axial beam asymmetry, the sail geometry must possess an inherent, passive stabilizing effect.

Sails that reflect high-energy beams are fundamentally distinct from solar sails, which exploit solar radiation pressure. Solar sails are envisioned as large Mylar or foil sheets supported by a truss structure, with a tethered spacecraft that also serves as ballast for the sail system. Some sail designs are mildly concave toward the radiation pressure.[16-19] For directed-energy sails, use of ballast hinders the objective of minimizing mass, and concave designs present insurmountable stability flaws, particularly during ~10 minute, >10 000 g acceleration phase of interstellar missions. Under these circumstances, convex sail designs possess good passive stability characteristics, without requiring ballast.

For example, consider a single-branch hyperboloid. Asymmetry in the directed energy beam would impart more momentum on one area of the sail than another, initiating a yaw in the direction of the higher force. As the yaw increases, the incident beam angle will move farther from the surface normal in the portion of the beam with higher intensity, which has the effect of lowering the effective torque in the area with higher intensity. At the same time, the incident angle will move closer to the surface normal in the portion of the beam with lower intensity, which has the effect of increasing the effective torque in that area. Therefore, changes in the incident beam angle due to yaw have the potential to passively counteract axial asymmetry of pressure. This fundamental property is illustrated in Fig. 1. This section explores passive stability properties of a 2D hyperbola under conditions of axially asymmetric pressure.

2.2. 2D Hyperbolic Segment

The parametric form of a hyperbola segment over a symmetric domain can be written as:

$$x = a \cdot \tan(s) \quad (a > 0) \qquad y = \frac{b}{\cos(s)} + c \quad (b < 0) \qquad s \in [-d, d] \tag{1}$$

For parameter values a = 1, b = –1 and d = 1, a (non-dimensional) hyperbola (lower branch) is shown in Fig. 1. The value of c is chosen to place the center of mass of the curve at the origin. The directed-energy beam is envisioned as vertical rays impinging on the top surface of the hyperbola. The wafer spacecraft would be situated in the concave portion of the hyperbola, protected from the directed-energy beam by the reflective sail.

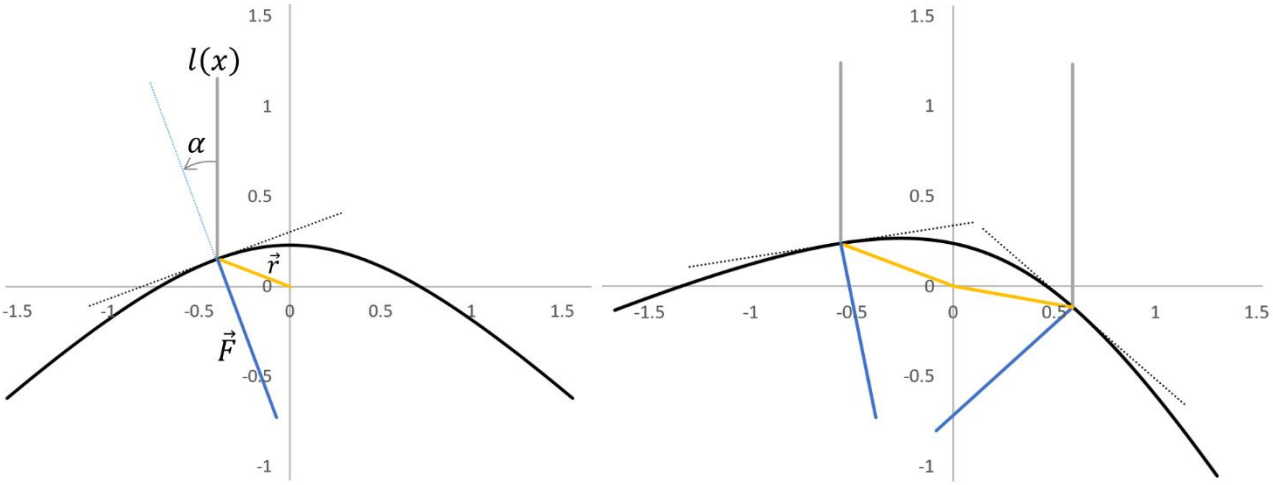

Figure 1. Left: Lower branch of a hyperbola, with center of mass at the origin. **Right:** The hyperbola is rotated about its center of mass, as might be caused by asymmetry in radiation pressure. Inherent passive stability is suggested by torque redistribution in the presence of yaw, resulting from increased or decreased momentum transfer when the angle of incidence moves toward or away from the surface normal, respectively.

The force imparted to the sail by the directed-energy beam is normal to the sail surface, as a pressure. Using the parametric form of Eq. (1), the tangent slope is calculated from the directional derivatives of the hyperbola:

$$\dot{x} = \frac{a}{\cos^2(s)} \qquad \dot{y} = \frac{b \cdot \sin(s)}{\cos^2(s)} \tag{2}$$

The angle between a vertical incident ray and the surface tangent normal (α) is calculated using the directional derivatives of Eq. (2):

$$\alpha = \operatorname{atan}\left(\frac{\dot{y}}{\dot{x}}\right) = \operatorname{atan}\left(\frac{b \cdot \sin(s)}{a}\right) \tag{3}$$

The torque on the sail at a given point (x, y) is calculated from the lever arm ($\vec{r}$) of the point, and the pressure force vector ($\vec{F}$) normal to the surface of the hyperbola at that point. The lever arm is a vector from the center of mass (x_{cm}, y_{cm}) to the point (x, y):

$$\vec{r} = \langle x - x_{cm}, y - y_{cm} \rangle = \langle a \cdot \tan(s), \frac{b}{\cos(s)} + c \rangle \tag{4}$$

With appropriate value of c selected in Eq. (1), the center of mass is at the origin. To model spatial asymmetry in the directed-energy beam (to account for imperfections in phase locking of multiple sources), the impinging force vector is scaled as some function $l(x)$ of lateral position in the incoming beam:

$$\vec{F} = [l(x) \cdot \cos(\alpha)] \cdot \langle \cos\left(\alpha + \frac{\pi}{2}\right), \sin\left(\alpha + \frac{\pi}{2}\right) \rangle \tag{5}$$

The torque magnitude is calculated from the length of the two vectors, and the angle between them:

$$\|\vec{\tau}\| = \left\|\vec{r} \times \vec{F}\right\| = \|\vec{r}\| \cdot \left\|\vec{F}\right\| \cdot \sin(\theta) \qquad \theta = \operatorname{acos}\left(\frac{\vec{r} \cdot \vec{F}}{\|\vec{r}\| \cdot \left\|\vec{F}\right\|}\right) \cdot \operatorname{sign}(-s) \tag{6}$$

The sign of the parameter value is useful for quadrant disambiguation of the arc-cosine function. The net torque on the sail is the sum of torques over the entire sail surface:

$$\tau_{\text{net}} = \int_{-d}^{d} \|\vec{\tau}\| ds \tag{7}$$

The hyperbola segment can be rotated about the center of mass, as might occur in response to asymmetric radiation pressure. The standard 2D rotation matrix is applied to the parametric form to rotate the hyperbola segment counter-clockwise through a positive angle ρ:

$$x' = a \cdot \tan(s) \cdot \cos(\rho) - \left(\frac{b}{\cos(s)} + c\right) \cdot \sin(\rho) \qquad y' = a \cdot \tan(s) \cdot \sin(\rho) + \left(\frac{b}{\cos(s)} + c\right) \cdot \cos(\rho) \tag{8}$$

Working with simple functions to describe the sail geometry (*e.g.*, a hyperbola) supports analytic derivative forms. The directional derivatives and incidence angle for the rotated hyperbola are:

$$\dot{x}' = \frac{a \cdot \cos(\rho) - b \cdot \sin(s) \cdot \sin(\rho)}{\cos^2(s)} \qquad \dot{y}' = \frac{a \cdot \sin(\rho) + b \cdot \sin(s) \cdot \cos(\rho)}{\cos^2(s)} \tag{9}$$

$$\alpha = \operatorname{atan}\left(\frac{a \cdot \sin(\rho) + b \cdot \sin(s) \cdot \cos(\rho)}{a \cdot \cos(\rho) - b \cdot \sin(s) \cdot \sin(\rho)}\right) \tag{10}$$

Table 1. Terms used for quantities presented in this section, with associated dimension.

Symbol	Interpretation	Dimension
a, b, c	Parameters of the hyperbola	[length]
s, d	Parametric variable for the hyperbola, and its range	non-dimensional
α	Beam Incidence Angle (to surface normal)	rad
$\vec{r}$	Lever-arm vector from center of mass to (x, y) on hyperbola	[length, length]
$\vec{F}$	Radiation pressure force vector at surface of hyperbola	[force/area]
θ	Angle between lever arm and radiation pressure	rad
$l(x)$	Intensity of directed-energy beam	[luminous intensity/length^2]
ρ	Yaw angle of the hyperbola	rad
$\vec{\tau}$	Torque vector acting on a point on the hyperbola	[length, length]

2.3. Static Equilibrium

The choice of a hyperbola for sail cross-section is based on the expectation that the design will passively counteract asymmetry of pressure, as a result of torque redistribution in the presence of yaw. The sail would be 'balanced' whenever the net torque over its surface is zero, indicating that the yaw angle is not being forced to change by the incident beam. A necessary condition for inherent passive stability is the existence of a zero-net torque state under realistic conditions of pressure axial asymmetry. As depicted in Fig. 1, the beam intensity force vector is modeled as some function $l(x)$ of lateral position x. Fig. 2 shows the net torque over a range of yaw angles for two beam intensity profiles. The first curve shows net torque for a uniform beam intensity, $l(x) = 1$. The graph shows a static equilibrium point at a yaw angle of 0. Using the hyperbola shown in Fig. 1, and beam intensity as $l(x) = 1 + 0.15x$, the beam intensity over the right half of the hyperbola will be higher than over the left half, initially causing a clockwise (negative) yaw. Under these conditions, Fig. 2. illustrates the existence of a static equilibrium point at a yaw of $\rho^* = -0.2$ radians. This result is consistent with inherent passive stability, since the initial negative yaw will push the spacecraft orientation toward the static equilibrium point that was originally induced by asymmetric pressure. Dynamic equilibrium analysis is discussed in §2.4.

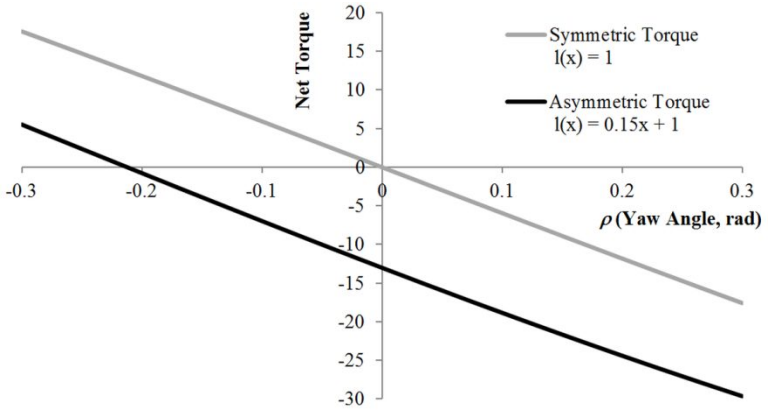

Figure 2. Analysis of static equilibrium points. The top curve confirms a static equilibrium at zero yaw angle under conditions of axially symmetric torque. The bottom curve suggests that negative yaw induced by asymmetric pressure will push the spacecraft orientation toward a static equilibrium point, consistent with the potential for inherent passive stability. Dynamic equilibrium analysis is presented in §2.4.

2.4. Dynamic Equilibrium

The dynamic stability of each static equilibrium point must be analyzed, for example using an appropriate energy method. A candidate Lyapunov function is identified using net torque:

$$V(\rho) = \frac{I \cdot \dot{\rho}^2}{2} + \rho \cdot \tau_{\text{net}}(\rho) \tag{11}$$

Based on Fig. 2, consider the point ρ^* where $\tau_{\text{net}}(\rho^*) = 0$, and for angles $|\rho - \rho^*| < \rho_{critical}$ that keep the hyperbola directrices from passing through horizontal. The hyperbola structure is locally stable at ρ^* whenever $\dot{V}(\rho^*) = 0$. Note that damping could also be introduced to the physical system, for example by incorporating photon-thruster or micro-reaction wheel attitude control on the spacecraft. The topic of damping will be considered in future work.

3. DIRECTED-ENERGY BEAM MODELS

3.1. Far-Field Beam Model: Magnitude of Asymmetry in the Beam

Thus far, analysis of sail stability has been presented in general terms for a specific sail geometry, without considering realistic forces on the sail, or the magnitude of asymmetry that might be expected in the directed-energy beam. In this section, a model is presented for beam formation by a coherently-combined laser array, based on previous work.[20] The model is suitable for estimating beam asymmetry, under some assumptions about the source of phase mis-alignment in a coherently-combined laser array. The interference pattern and resulting far-field intensity distribution of

multiple emitters in a phased-array design can be determined by scalar diffraction theory. The complex far-field amplitude for a flat, linear array of emitters in phase alignment is given by:

$$E(\theta) = E_0 \cdot \frac{e^{[i \cdot k \cdot a \cdot sin(\theta)]} - 1}{i \cdot k \cdot sin(\theta)} \cdot \sum_{p=0}^{N-1} e^{[i \cdot k \cdot p \cdot d \cdot sin(\theta)]} \tag{12}$$

Given the complex amplitude, the far-field beam intensity for the linear array is then:

$$I(\theta) = |E(\theta)|^2 \tag{13}$$

For a 1-D linear array, the far-field beam intensity for a square array with beam intensity $I_x(\theta)$ along one axis and $I_y(\psi)$ along a perpendicular axis is:

$$I(\theta, \psi) = I_x(\theta) \cdot I_y(\psi) \tag{14}$$

Eq. (12) assumes perfect mechanical alignment, as well as perfect frequency, amplitude and phase control for every emitter in the array. A simulation was performed, based on Eqs. (12)-(14) for a 5 by 5 square array. Fig. 3 shows 1-D and 2-D far-field beam patterns.

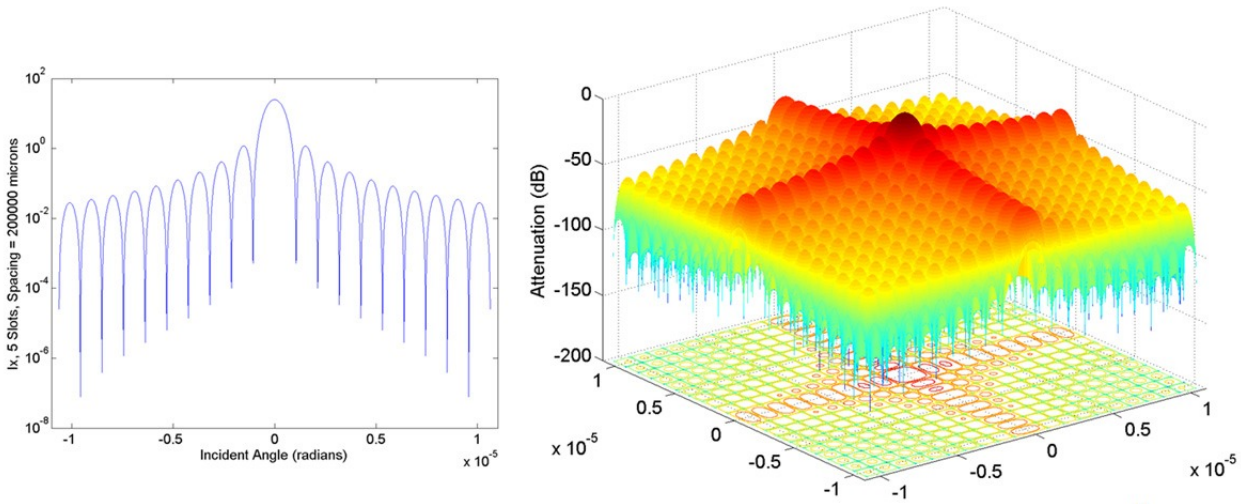

Figure 3. Baseline simulation results for a 5 by 5 close-packed array of square emitters in phase alignment.[20] Each emitters is a 20 cm by 20 cm square ($a = d = 20$ cm), so total aperture is 1 m, $N = 25$, and the nominal emitter frequency is set to $\lambda = 1.06$ μm. These results would only be attained by having perfect mechanical alignment and perfect frequency, amplitude and phase control of every emitter in the array.

Table 2. Terms used for simulations presented in this section, with associated dimension or units.

Symbol	Interpretation	Dimension, units
λ	Nominal emitter wavelength	μm
d	Nominal element spacing (array pitch)	μm
θ	Angular variable (viewing angle away from normal to emitter array plane)	rad
E	Complex far-field amplitude	V/m
I	Far-field beam intensity	W/m^2
k	$2\pi/\lambda$	μm^{-1}
a	Aperture opening size	μm
N	Number of emitters in a single dimension of an array	dimensionless

The model can be modified to include additive fixed and time-varying phase misalignments. such as might be induced by structural misalignment, mechanical vibration or thermal variations. The complex far-field amplitude for a linear array of emitters with static (E_f) and time-varying (E_t) phase misalignments at each emitter is given by:

$$E(\theta, t) = \frac{e^{[i \cdot k \cdot a \cdot sin(\theta)]} - 1}{i \cdot k \cdot sin(\theta)} \cdot \sum_{p=0}^{N-1} e^{\{i \cdot [k \cdot p \cdot d \cdot sin(\theta) + E_f(p) + E_t(p,t)]\}} \tag{15}$$

For simulations, fixed phase differences are drawn randomly from a normal distribution with zero mean and a specified standard deviation. Standard deviation represents the variation among fixed alignment differences, and is typically stated in terms of a fraction of a single cycle at the nominal emitter frequency. Fixed alignment differences can be chosen randomly, since they can be viewed as un-correlated random errors. However, time-varying terms can be both correlated and uncorrelated. Vibrational modes in the structure will create phase misalignments that are correlated among the array emitters. Additional perturbations are also possible, for example due to thermal changes in optical paths or non-linear reactions of optical elements to structural vibrations. Some of these scenarios may result in uncorrelated phase misalignments, which can also be included in the model by adding a series of time-varying terms, *i.e.*, $E_t(p, t)$ in Eq. (15) can be a sum representing several components.

The simulation results shown in Fig. 4 represent a laser phased array that includes fixed phase mis-alignments (E_f) at each emitter with a 1σ error of $\lambda/8$. Comparison of these results to Fig. 3 shows significant beam degradation, with significant power moving from the main peak to side lobes. Also evident is a pointing shift, *i.e.*, the main lobe axis is no longer aligned with the array axis, with a pointing error on the order of 1 μrad.

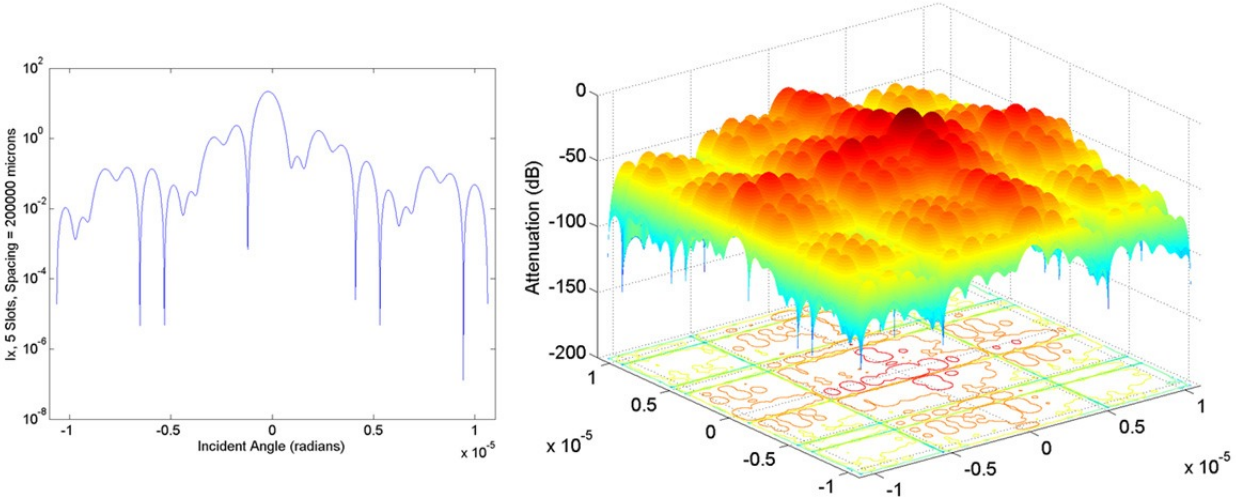

Figure 4. Simulation results for a 5 by 5 close-packed array of emitters with static phase perturbations.[20] Again, emitters are modeled as $a = d = 20$ cm, total aperture is 1 m, and the nominal emitter frequency is set to 1.06 μm (compare to Fig. 3). Mis-alignments were randomly assigned to each emitter, with magnitudes drawn from a normal distribution with $1\sigma = 2\pi/8$.

4. THE PHYSICS OF LIGHT-MIRROR INTERACTION

4.1. Modeling Objectives

Flux on the sail will be immense, so it is imperative to develop a realistic model for the interaction between the directed-energy beam and the reflective sail. Numerous papers describing light-matter interaction in various scenarios are available.[21-31] Light matter interactions in increased order of sophistication can be described using classical, semi-classical and fully quantum mechanical approaches. In the classical approach, the light field is described by Maxwell's equations, matter as a collection of simple harmonic oscillators in the dipole approximation and light-matter interactions are a result of resonant coupling of the light field resonantly interacting with the electric charge of the atomic system. In the semi-classical approach, the matter field is quantized while the light field is represented by classical amplitudes and the interaction is given by the Rabi model. In the fully quantum picture both light and matter fields are quantized and the interaction is specified by the Jaynes-Cummings model.[32-35]

Exchange of energy and momentum occurs when light scatters from a mirror. Assuming a closed system, the incident photon imparts kinetic momentum to the mirror. The resultant mechanical motion of the mirror can be modeled with various degrees of sophistication, ranging from the particle collision model to the fully quantized scattering model. We are primarily interested in the transfer of energy and momentum from the light field to the reflecting sail. A purely mechanical model is described in the next section.

4.2. A Baseline Non-Relativistic Model

As a baseline approach, the directed energy beam incident on the reflective sail is modeled as a pure mechanical collision of rigid objects in the non-relativistic limit. Consider an incoming photon with linear momentum p impinging on a mirror at an angle of incidence α and at distance d from the mirror's center of mass, as shown in Fig. 5. In addition to imparting a horizontal kick to the mirror, the reflection also causes the mirror to rotate about its center of mass with an angular velocity $\omega = \dot{\theta}$. Conservation equations for linear and angular momenta are:

$$p_l \cdot \cos(\alpha) = -p_l{}' \cdot \cos(\beta) + M \cdot \Delta v_{cm} \tag{16}$$

$$p_l \cdot \sin(\alpha) = -p_l{}' \cdot \sin(\beta) \tag{17}$$

$$L_l = L_l' + I \cdot \Delta\omega \tag{18}$$

Assuming the change in angular momentum of the photon is purely extrinsic:

$$p_l \cdot d \cdot \cos(\alpha) = -p_l{}' \cdot d \cdot \cos(\beta) + I \cdot \Delta\omega \tag{19}$$

The mechanical energy is:

$$p_l \cdot c = p_l' \cdot c + \Delta KE_t + \Delta KE_r \tag{20}$$

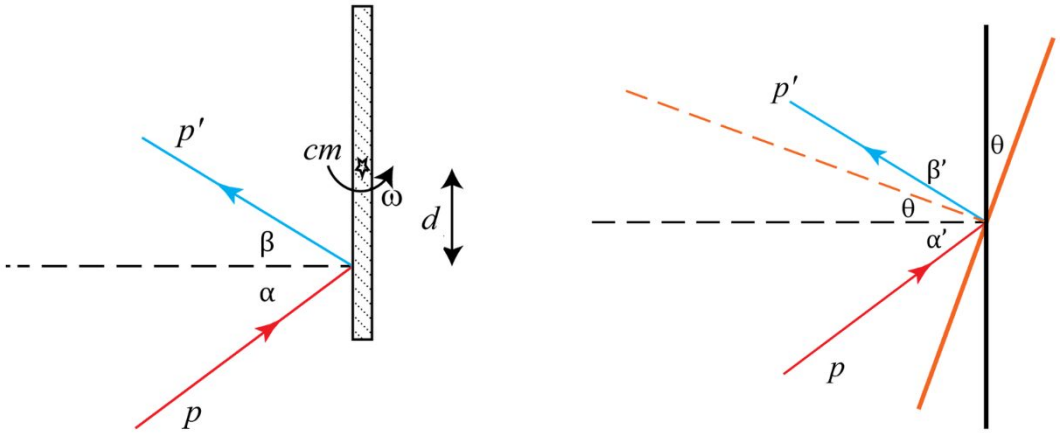

Figure 5. Schematic diagram of light-mirror interaction as modeled for this study. **Left:** A photon reflected by a stationary mirror. **Right:** n^{th} scattering.

Table 3. Terms used for simulations presented in this section, with associated dimension or units.

Symbol	Interpretation	Dimension, units
p	Linear momentum of the incident photon	kg m/s
p'	Linear momentum of the reflected photon	kg m/s
p_m	Linear momentum of the mirror	kg m/s
α	Photon angle of incidence	rad
β	Photon angle of reflection	rad
ω	Angular velocity of the mirror about its center of mass (c.m)	rad/s
d	Length of the "lever arm"	m
cm	Visual representation of the center of mass of the mirror	-
M	Mass of the mirror	kg

Now consider a more general case, where the mirror has already rotated by θ after receiving a kick from a single photon. For the incoming photon, the angles of incidence and reflection are transformed as $\alpha \rightarrow \alpha + \theta$, $\beta \rightarrow \beta - \theta$ and $\omega = \dot{\theta}$. With each reflection, the *mirror* experiences both linear and angular acceleration.

4.3. Discussion of Limitations in the Mechanical Model

While the mechanical photon collision model captures the essential mechanics of the situation, it is likely too simplistic to describe all of the important phenomena when a high-energy directed-energy beam strikes a reflective mirror. Working toward a more complete model, the transfer of energy and momentum from a field to matter can be

described in terms of *densities* and the interaction with matter is encapsulated in by a *stress tensor*. There are two forms of the stress tensor, the so-called Minkowski and Abraham forms, derived directly from their respective expressions for momentum density of light *within* a medium. It is not yet clear which form is correct for the present scenario, although there seems to be a consensus on interpreting the Minkowski momentum as the recoil momentum of the atom interacting with the photon, while the Abraham momentum is interpreted as the field. Some authors have suggested that the choice of description is experimentally driven, a pushing force suggests use of the Abraham form, while a pulling force the Minkowski form.[52] A thorough description of the various arguments is available.[29,38-42, and references therein] In addition, it may also be necessary to consider the canonical momentum of light in a dielectric to obtain a more complete picture of the interactions.[43-45] A useful model must be consistent with at least one of these established theories.

5. A 3D MULTI-PHYSICS MODEL SAIL CONCEPT

5.1. Hyperboloid

The preceding 2D analysis demonstrated that a hyperbola displays inherent passive stabilization properties under conditions of pressure axial asymmetry. A long-term goal of this research is to build a 3D multi-physics model of a hyperboloid sail, incorporating boundary conditions and forcing terms based on realistic values of radiative flux, flux asymmetry, and light-mirror interaction described as physical models in the preceding sections. The image in Fig. 6 shows results from the first iteration of a COMSOL model. The model includes a sail geometry (hyperbola), with a circular wafer mounted 'leeward' within the sail cavity. At the current time, the model is 'anchored' at the center of mass, rather than 'free'. Choices for sail thickness and material properties are arbitrary, at this point. The model in its current form could be used to explore rotational forces on a reaction wheel. The current iteration has no laser; force on the sail is modeled as a pressure, normal to the sail surface. The same type of function used in the 2D model was incorporated in the 3D model to add asymmetry to the pressure, in this case $l(x) = 1+0.01x$.

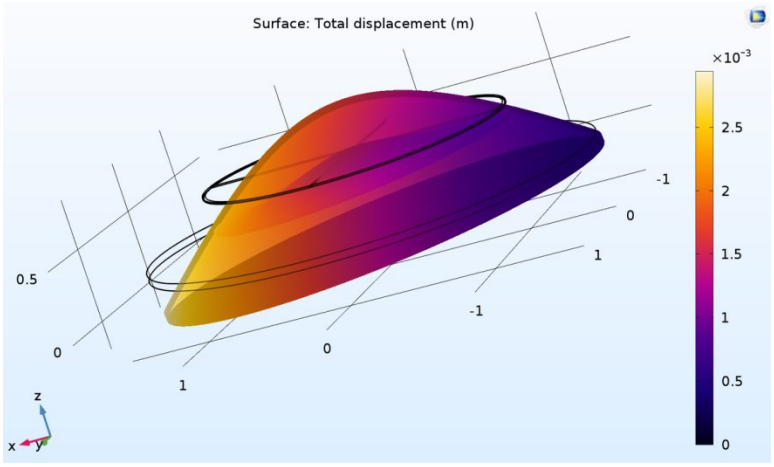

Figure 6. 3D model of a conceptual hyperboloid sail. The wafer-scale spacecraft is supported within the sail cavity. Asymmetric flux is imparted to the sail, inducing a yaw. The sail outline shows deviations from the unconstrained position depicted by the solid lines. Steady-state orientation is indicative of inherent passive stability.

6. CONCLUSIONS

6.1. Progress to Date

Wafer-scale spacecraft are envisioned to begin interstellar missions in low-Earth orbit, accelerated to relativistic speeds (>0.1 *c*) by a directed-energy beam pushing the spacecraft's reflective sail. The aim of research presented in this paper is to analyze the stability of reflective sail designs within the context of accelerating wafer-scale spacecraft to relativistic speeds. Fluctuations and asymmetry in the beam will create rotational forces on the sail, so the sail geometry must possess an inherent, passive stabilizing effect. A hyperboloid shape is proposed, since changes in the incident beam angle due to yaw will passively counteract rotational forces, the result of torque redistribution in response to yaw. A 2D

hyperbolic cross-section was analyzed for static equilibrium, confirming the passive stabilizing effect. A dynamic analysis using a candidate Lyapunov function confirms stability of the static equilibrium position. The next goal is to incorporate realistic boundary conditions and forcing in the dynamic model. A directed-energy beam far-field intensity model is used to model beam intensity and asymmetry at the spacecraft. Fundamental physics of light-mirror interaction are adapted for the spacecraft acceleration scenario, yielding a model of basic forces on the mirror. Simulations of the beam and light-mirror models provide more realistic input to a 3D multi-physics model of a reflecting hyperboloid sail. Initial results from a preliminary 3D multi-physics model support the conjecture of passive stability, although much development remains to achieve a realistic 3D simulation.

6.2. Considerations for Additional Study

As the spacecraft moves away from Earth, the beam flux will decrease asymptotically to zero, leaving the spacecraft to coast through most of its journey. Final velocity will be attained within ~1 AU of Earth, depending on the optical properties of the laser array, requiring massive acceleration during the initial stage of the long journey. Many issues related to spacecraft stability remain to be studied. This paper considers a hyperboloid, and concludes that the design possesses some traits of inherent passive stability. The hyperboloid curvature must be optimized for expected beam conditions, since higher curvature increases stability, but reduces effective thrust. A hyperboloid sail could be optimized by seeking the minimum curvature that is stable over the expected range of beam asymmetries. Additionally, sail geometry optimization could consider other shapes that could potentially be more efficient and/or stable than a hyperboloid. The current beam intensity model is a far-field estimate, but it is clear that a near-field model will be required.[46] Dynamic stability studies should consider damping forces, such as could be provided by photon-thruster or micro-reaction-wheel attitude control systems. Mechanical design of the spacecraft, and material choices, will clearly have important effects on stability, since mechanical deformation due to structural and acoustic modes will affect sail shape.[47-48] Flux on the sail will be immense, so imperfect reflectance will be a major issue. Dielectric sails show promise. Absorption in the sail material will result in thermal expansion, altering properties of the mechanical design. Thermal management will be critical. Waste heat could potentially be recycled as a power source, *e.g*. for attitude control. As the spacecraft accelerates to relativistic speeds, the directed energy beam will be red-shifted, so reflectance properties of the sail material must be considered over a wide frequency range. Additionally, reflection from the relativistic sail will change character, with a significant effect on thrust.[49-51]

ACKNOWLEDGEMENTS

We gratefully acknowledge funding from the NASA California Space Grant NASA NNX10AT93H in support of this research. We also gratefully acknowledge funding from the NASA Innovative Advanced Concepts grant NNH15ZOA001N in support of this research.

REFERENCES

[1] Marx, G., "Interstellar vehicle propelled by terrestrial laser beam," *Nature* 211, 22-23 (1966).

[2] Redding, J. L. "Interstellar vehicle propelled by terrestrial laser beam," *Nature* 213, 588-589 (1967).

[3] Matloff, G.L. and Mallove, E., "Solar sail starships: the clipper ships of the galaxy," *Journal of the British Interplanetary Society*, v. 34, pp.371-380 (1981).

[4] Forward, R. L., "Roundtrip interstellar travel using laser-pushed lightsails," *Journal of Spacecraft and Rockets*, v. 21, 187-195 (1984).

[5] Beals, K. A., Beaulieu, M., Dembia, F. J., Kerstiens, J., Kramer, D. L., West, J. R., and Zito, J. A., "Project Longshot: An Unmanned Probe to Alpha Centauri," US Naval Academy, NASA-CR-184718, (1988).

[6] Crawford, I.A., "Interstellar travel: a review for astronomers," *Quarterly Journal of the Royal Astronomical Society*, v. 31, pp.377-400 (1990).

[7] Simmons, J.F.L. and McInnes, C.R., "Was Marx right? or How efficient are laser driven interstellar spacecraft?," *American Journal of Physics*, 61(3), pp.205-207 (1993).

[8] Taylor, T., Anding, R.C., Halford, D. and Matloff, G.L. "Space based energy beaming requirements for interstellar laser sailing," *Beamed Energy Propulsion: First International Symposium on Beamed Energy Propulsion,* 664(1), pp. 369-381 (2003).

[9] Long, K.F., *Deep Space Propulsion: A Roadmap to Interstellar Flight*. Springer Science & Business Media (2011).

[10] Bae, Y. K., "Prospective of photon propulsion for interstellar flight," *Physics Procedia* 38, 253-279 (2012).

[11] Bible, J., Bublitz, J., Johansson, I.E., Hughes, G.B., and Lubin, P. "Relativistic Propulsion Using Directed Energy," *Nanophotonics and Macrophotonics for Space Environments VII*, edited by Edward W. Taylor, David A. Cardimona, Proc. of SPIE, Vol. 8876, 887605 (2013).

[12] Lubin, P., Hughes, G.B., Bible, J., Bublitz, J., Arriola, J., Motta, C., Suen, J., Johansson, I., Riley, J., Sarvian, N., Clayton-Warwick, D., Wu, J., Milich, A., Oleson, M., Pryor, M., Krogen, P., Kangas, M., and O'Neill, H. "Toward Directed Energy Planetary Defense," *Optical Engineering*, Vol. 53, No. 2, pp. 025103 1-18 (2014).

[13] Lubin, P., Hughes, G.B., Bible, J. and Johansson, I. "Directed Energy for Planetary Defense and Exploration: Applications to Relativistic Propulsion and Interstellar Communications," *Journal of the British Interplanetary Society*, vol. 68, no. 5/6, pp. 172-182 (2015).

[14] Lubin, P. "A Roadmap to Interstellar Flight," arXiv:1604.01356v5 [astro-ph.EP] (2016).

[15] Kare, J.T. "High acceleration micro-scale laser sails for interstellar propulsion," *Final Report, NIAC Research Grant*, pp.07600-070 (2002).

[16] McInnes, C.R. Solar sail design. In *Solar Sailing* (pp. 56-111), Springer London (1999).

[17] Gaspar, J., Mann, T., Behun, V., Wilkie, W.K. and Pappa, R. "Development of modal test techniques for validation of a solar sail design", *AIAA*, *1665*, p.45 (2004).

[18] Leipold, M., Eiden, M., Garner, C.E., Herbeck, L., Kassing, D., Niederstadt, T., Krüger, T., Pagel, G., Rezazad, M., Rozemeijer, H. and Seboldt, W. "Solar sail technology development and demonstration", *Acta Astronautica*, 52(2), pp.317-326 (2003).

[19] Greschik, G. and Mikulas, M.M. "Design study of a square solar sail architecture", *Journal of Spacecraft and Rockets*, 39(5), pp.653-661 (2002).

[20] Hughes, G.B., Lubin, P., Griswold, J., Bozinni, D., O'Neill, H., Meinhold, P., Suen, J., Bible, J., Riley, J., Johansson, I., Pryor, M. and Kangas, M. "Optical modeling for a laser phased-array directed energy system," *Nanophotonics and Macrophotonics for Space Environments VIII*, edited by Edward W. Taylor, David A. Cardimona, Proc. of SPIE, Vol. 9226 (2014).

[21] Barnett, S.M. and Loudon, R., "The enigma of optical momentum in a medium," *Philosophical Transactions of the Royal Society of London A: Mathematical, Physical and Engineering Sciences*", 368(1914), pp.927-939 (2010).

[22] Mansuripur, M., "Radiation pressure and the linear momentum of the electromagnetic field," *Optics Express*, 12(22), pp.5375-5401 (2004).

[23] Požar, T., "Oblique reflection of a laser pulse from a perfect elastic mirror," *Optics letters*, *39*(1), pp.48-51 (2014).

[24] Požar, T. and Možina, J., "1D problems of radiation pressure on elastic solids," *Optical Trapping and Optical Micromanipulation XII*, edited by Kishan Dholakia, Gabriel C. Spalding, Proc. of Vol. 9548, 95480N (2015).

[25] Martelli, P. and Martinelli, M., "Representation and Evolution of the Angular Momentum of the Light," *IEEE Photonics Journal*, 6(4), pp.1-9 (2014).

[26] Alam, M.S. and Chowdhury, M.D., "Study of reflection of light by a moving mirror," *Indian Journal of Physics*, 83(2), pp.233-240 (2009).

[27] Gjurchinovski, A., "Reflection from a moving mirror—a simple derivation using the photon model of light," *European Journal of Physics*, 34(1), p. L1 (2012).

[28] Castaños, L.O. and Weder, R., "Classical dynamics of a moving mirror due to radiation pressure," *Journal of Physics: Conference Series*, Vol. 512, No. 1, p. 012005 (2014).

[29] Bolotovskiĭ, B.M. and Stolyarov, S.N., "Reflection of light from a moving mirror and related problems," *Physics-Uspekhi*, 32(9), pp.813-827 (1989).

[30] Baxter, C., Babiker, M. and Loudon, R., "Canonical approach to photon pressure," *Physical Review A*, 47(2), p.1278 (1993).

[31] Aharonov, Y., Botero, A., Nussinov, S., Popescu, S., Tollaksen, J. and Vaidman, L., "The classical limit of quantum optics: not what it seems at first sight," *New Journal of Physics*, 15(9), p.093006 (2013).

[32] Scully, M.O. and Zubairy, M. S. *Quantum Optics*, Cambridge Univ. Press (1997).

[33] Boyd, R. *Nonlinear Optics*, Elsevier Science (2013).

[34] Knight, P. L. and Allen, L. *Concepts of Quantum Optics*, Elsevier Science (2013).

[35] Grynberg, G., Aspect, A., Fabre, C. and Cohen-Tannoudji, C.. *Introduction to Quantum Optics: From the Semi-classical Approach to Quantized Light*, Cambridge University Press (2010).

[36] Allen, L., Beijersbergen, M.W., Spreeuw, R.J.C. and Woerdman, J.P. "Orbital angular momentum of light and the transformation of Laguerre-Gaussian laser modes," *Physical Review A*, 45(11), p.8185 (1992).

[37] Padgett, M. In: *Proc. Int Optical MEMS and Nanophotonics (OMN) Conf.*, pp. 71–72 (2014).

[38] Milonni, P.W. and Boyd, R.W. "Momentum of light in a dielectric medium," *Advances in Optics and Photonics*, 2(4), pp.519-553 (2010).

[39] Pfeifer, R.N., Nieminen, T.A., Heckenberg, N.R. and Rubinsztein-Dunlop, H. "Colloquium: Momentum of an electromagnetic wave in dielectric media," *Reviews of Modern Physics*, 79(4), p.1197 (2007).

[40] Bradshaw, D.H., Shi, Z., Boyd, R.W. and Milonni, P.W. "Electromagnetic momenta and forces in dispersive dielectric media," *Optics Communications*, 283(5), pp.650-656 (2010).

[41] Barnett, S.M., "Resolution of the Abraham-Minkowski dilemma," *Physical Review Letters*, 104(7), p.070401 (2010).

[42] Mansuripur, M., "Resolution of the Abraham–Minkowski controversy," *Optics Communications*, 283(10), pp.1997-2005 (2010).

[43] Baxter, C., Babiker, M. and Loudon, R. "Canonical approach to photon pressure," *Physical Review A*, 47(2), p.1278 (1993).

[44] Garrison, J.C. and Chiao, R.Y. "Canonical and kinetic forms of the electromagnetic momentum in an ad hoc quantization scheme for a dispersive dielectric," *Physical Review A*, 70(5), p.053826 (2004).

[45] Dodin, I.Y. and Fisch, N.J. "Axiomatic geometrical optics, Abraham-Minkowski controversy, and photon properties derived classically," *Physical Review A*, 86(5), p.053834 (2012).

[46] Ruffner, D.B. and Grier, D.G. "Optical forces and torques in nonuniform beams of light," *Physical review letters*, 108(17), p.173602 (2012).

[47] Mansuripur, M., "Light-matter interaction: conversion of optical energy and momentum to mechanical vibrations and phonons," *Quantum Sensing and Nano Electronics and Photonics XIII*, edited by M. Razeghi, G.J. Brown, and J.S. Lewis, Proc. of SPIE, Vol. 9755, 975521 (2016).

[48] Sgattoni, A., Sinigardi, S., Fedeli, L., Pegoraro, F. and Macchi, A. "Laser-driven Rayleigh-Taylor instability: Plasmonic effects and three-dimensional structures," *Physical Review E*, *91*(1), p.013106 (2015).

[49] Galli, J.R. and Amiri, F., "A general principle for light reflecting from a uniformly moving mirror: A relativistic treatment," *American Journal of Physics*, *80*(8), pp.680-683 (2012).

[50] Goedecke, G., Toussaint, V. and Cooper, C., "On energy transfers in reflection of light by a moving mirror," *American Journal of Physics*, 80(8), pp.684-687 (2012).

[51] Corrêa, R. and Saldanha, P.L., "Photon reflection by a quantum mirror: A wave-function approach," *Physical Review A*, 93(2), p.023803 (2016).

[52] Zhang, L., She W., Peng N. and Leonhardt U., "Experimental evidence for Abraham pressure of light", *New Journal of Physics*, Volume 17, (2015).